Materials Advances

ROYAL SOCIETY OF CHEMISTRY

PAPER

View Article Online
View Journal | View Issue

Cite this: *Mater. Adv.*, 2026, 7, 886

Tuning the radiation tolerance of titanate pyrochlore *via* Sn-substitution: an *in situ* ion irradiation study of pyrochlore-glass ceramics

Mohamed Ruwaid Rafiuddin, *[ab] Anamul Haq Mir, *[a] Linggen Kong [b] and Yingjie Zhang [b]

The high-level radioactive waste stream resulting from the reprocessing of spent nuclear fuel compriseslong-lived actinides and processing chemical impurities. Glass-ceramics (GCs) are being proposed as a potential candidate to host the actinides and processing impurities in the crystalline and glass phases, respectively. Some of the ceramics considered for actinide immobilization are pyrochlores ($Ln_2B_2O_7$; Ln = lanthanides and Y, B = Ti, Sn, Zr, and Hf) and in the present study, the pyrochlore GCs ($Y_2Ti_{2-x}Sn_xO_7$ and Ln_2TiSnO_7) have been synthesized and their response to ion-irradiation (600 keV Xe^{2+}) has been investigated under *in situ* conditions using transmission electron microscopy (TEM). The primary focus of this study is the effect of Sn-substitution into the B-site of the pyrochlore structure on the radiation tolerance of these materials. With an increase in Sn-substitution, the materials become increasingly radiation tolerant as indicated by the higher ion-fluences required for amorphization. The fully Sn-substituted pyrochlore was determined to be ~25 times and ~78 times more radiation tolerant than its Ti-counterpart at 143 K and 298 K, respectively. Similarly, Sn-rich pyrochlores were determined to have a critical temperature (T_c) of amorphization ~3 times lower than that of the Ti-rich materials. The improved radiation tolerance of Sn-substituted pyrochlores is a result of the interplay of structure, energetics, and the nature of the Ln–O and B–O bonds. This study has demonstrated that in terms of radiation tolerance, the stannate pyrochlore GC is an attractive candidate for HLW immobilization over titanate counterparts.

Received 10th June 2025,
Accepted 30th September 2025

DOI: 10.1039/d5ma00619h

rsc.li/materials-advances

1. Introduction

To combat the adverse effects of greenhouse gas emissions, many countries are aiming to transition into a low carbon economy by opting for carbon-free energy sources such as nuclear energy for electricity generation.[1] Though nuclear energy has a low carbon footprint, it does generate spent nuclear fuel (SNF) comprising long-lived radionuclides (*e.g.*, Pu, Np, Am, Cm, *etc.*). Long-term plans are proposed in some countries for the immobilization of these radionuclides in stable waste forms, followed by storage and final disposal in a geological repository.[2] The choice of the nuclear waste form (*e.g.*, glass, ceramics, and glass-ceramics (GCs)) is dependent on the chemistry of the waste stream.[3] Among the candidate waste forms, pyrochlore ceramics ($A_2B_2O_7$, A = actinide (An), lanthanide (Ln), Y; B = Ti, Zr, Hf, and Sn; space group: $Fd\bar{3}m$) are proposed as potential candidates owing to their superior chemical durability for the immobilization of high-level waste (HLW) comprising tetravalent Np and Pu, and trivalent minor actinides (*e.g.*, Np, Am, and Cm).[4] However, they cannot accommodate the wide range of processing chemicals and impurities (which are typically found in the HLW stream) in their crystal structures.[5] To circumvent this issue, GC composite materials are designed to accommodate actinides in durable ceramics while fission products, processing chemicals, and impurities can be contained in the glass phase.[5–7] Pyrochlore based GCs contain pyrochlore crystals distributed within the glass phase and thus combine the simple processing and chemical flexibility of glasses with the superior chemical durability of the ceramics for the immobilization of actinide-rich waste streams.[7,8]

Materials adopting the pyrochlore structure ($A_2B_2O_7$) crystallize in a cubic crystal system (space group: $Fd\bar{3}m$) and are closely related to the fluorite structure (AO_2; space group: $Fm\bar{3}m$) in which the pyrochlore is an O deficient superstructure of the fluorite and has a unit cell almost double the size of the fluorite.[4] The crystal structure of a representative pyrochlore ($Y_2Ti_2O_7$) is provided in Fig. 1. The A-site cation is occupied by the larger trivalent lanthanide and yttrium ions and is

[a] *MIAMI Facility, School of Computing and Engineering, University of Huddersfield, Huddersfield, UK. E-mail: a.h.mir@hud.ac.uk*
[b] *Australian Nuclear Science and Technology Organisation, Locked Bag 2001, Kirrawee DC, NSW 2232, Australia. E-mail: rafiuddr@ansto.gov.au*

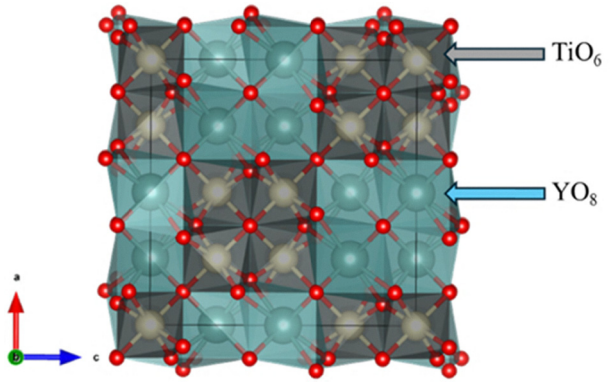

Fig. 1 Crystal structure of the $Y_2Ti_2O_7$ pyrochlore with the YO_8 and TiO_6 polyhedra shown in teal and grey generated using VESTA software.[14]

coordinated to eight oxygen atoms, whereas the B-site cation is occupied by the smaller cations (*e.g.*, Ti, Zr, Hf, and Sn), which are coordinated to six oxygen atoms.[9] The structure consists of three oxygen sites (O1 = 48f, O2 = 8b, and O3 = 8a) and of these three sites, two are occupied (O1 = 48f and O2 = 8b) and the third site is vacant (O3 = 8a).[10,11] Six oxygens occupy the O1 site and are coordinated to two A-site and two B-site cations, while the seventh oxygen occupies the O2 site and are coordinated to four A-site cations.[11] The vacant O3 site is coordinated to four B-site cations.[11] In the ideal pyrochlore structure, the cations and oxygen vacancies are ordered.[12] Kong *et al.* showed that the pyrochlore structure can undergo a structural transformation to a defect fluorite *via* compositional tuning.[13] In that study, the $Y_2Hf_xTi_{2-x}O_7$ ($0 \leq x \leq 2.0$) system was investigated and it was shown that the pyrochlore transformed to defect fluorite for compositions $x = 1.7$ and 2.0.[13] A defect fluorite structure is an oxygen deficient derivative of the fluorite structure, with the cations and oxygen being disordered.[4] The x positional parameter of the O_{48f} oxygen determines the deviation from the ideal fluorite structure and in a completely defect fluorite structure, the O_{48f} is shifted towards the B-site ion by $x = 0.375$.[4] In a defect fluorite structure, the seven oxygen atoms are randomly distributed over O1, O2, and O3 sites.[13]

Ceramic wasteforms will experience self-radiation damage from the α-decay of the incorporated actinides and may eventually transform from the crystalline to amorphous state.[15] The effects of radiation on the pyrochlore structure have been studied either by self-irradiation (*via* doping of short-lived actinides such as ^{244}Cm with a half-life of 18.1 years) or by external irradiation (*via* using high energy ion beams).[16–19] Earlier studies on actinide incorporated pyrochlores ($(Nd_{0.85}Cm_{0.15})_2(Ti_{1.65}Zr_{0.35})O_7$ and $(Gd,Cm)_2Ti_2O_7$) have shown the structural transformation from the crystalline to amorphous state as a result of self-irradiation.[4] In the $(Gd,Cm)_2Ti_2O_7$ system, the material amorphized at a dose of 3.1×10^{18} α-decay events per gram, resulting in a macroscopic swelling of 5% and an increase by a factor of 20–50 in the dissolution rate of Cm.[4,20] These studies have demonstrated that radiation can affect both the structure and as a result, the chemical durability of the pyrochlore based waste forms.[4,16]

Though self-irradiation experiments offer a real insight into the radiation experienced by the nuclear waste form, they are generally time-consuming and requires radioactive materials.[15] Ion beam irradiation experiments, on the other hand, offer a convenient route to accelerate the radiation damage process by simulating the α-decay process using high energy non-radioactive ion beams.[15,21] These experiments have been carried out on a wide variety of titanate pyrochlore compositions (*e.g.*, $Ln_2Ti_2O_7$, Ln = La–Lu, and Y) and results suggest that these materials are susceptible to radiation-induced crystalline to amorphous transformation.[19,22–24]

Most titanate pyrochlores can be amorphized upon high-energy ion irradiation and hence, efforts have been made to design materials with increased radiation tolerance *via* compositional tuning.[23,25] In the literature, it has been demonstrated that the disordered pyrochlores (*i.e.*, defect fluorite-type) exhibit higher radiation resistance than the ordered pyrochlores.[26] Materials with defect fluorite-type structure are typically obtained through the substitution of B-site cations (*e.g.*, substitution of Ti with Zr, Hf *etc.*).[27] Some of the compositions with defect fluorite structure include $Ln_2Zr_xTi_{2-x}O_7$ and $Y_2Hf_xTi_{2-x}O_7$.[13,28,29] Sickafus *et al.* compared the radiation response of the ordered pyrochlore ($Er_2Ti_2O_7$) and the defect-fluorite ($Er_2Zr_2O_7$) when subjected to 350 keV Xe^{2+} ions up to a fluence of 1×10^{16} ions per cm^2.[26] It was shown that $Er_2Ti_2O_7$ could be amorphized at a lower ion fluence while $Er_2Zr_2O_7$ remained crystalline at high Xe^{2+} ion fluences thus highlighting the radiation resistant behaviour of defect fluorites.[26] Similar observations were made by Wang *et al.* on $Gd_2Zr_xTi_{2-x}O_7$ ($x = 0$, 0.25, 0.5, 0.75, and 1) and it was shown that with an increase in Zr content, the material becomes radiation resistant when subjected to 1 MeV Kr^+ ion beam.[30] In that study, the critical amorphization temperatures (*i.e.*, T_c – the temperature above which amorphization does not occur) of $Gd_2Ti_2O_7$ and Zr-rich compositions ($x > 0.5$) were 1100 K and 380 K, respectively.[30] In a typical geological repository, the temperatures are expected to be ~320–400 K and hence, Zr-rich pyrochlore with a lower T_c (380 K) can be expected to remain crystalline.[30,31] However, higher processing temperatures are generally required for the synthesis of Zr-rich pyrochlores.[32]

Stannate pyrochlores in which the tin occupies the B-site of the pyrochlore have also been shown to be more radiation resistant than titanate pyrochlores.[33,34] Yudintsev *et al.* investigated the radiation stability of Cm-doped stannate pyrochlore ($(Gd_{1.891}Cm_{0.091}Pu_{0.013})Sn_2O_7$) and found that at room temperature, this material amorphized at a dose of $\sim 10^{19}$ α-decay per g which is ~2–5 times higher than those required for amorphization of Cm-doped titanate ($(Gd,Cm)_2Ti_2O_7$) and zirconate ($(Gd_{1.935}Cm_{0.065})TiZrO_7$) pyrochlores.[35] Lumpkin *et al.* investigated the tin substituted pyrochlore ($Y_2Sn_xTi_{2-x}O_7$) system and monitored their radiation response to a 1 MeV Kr ion beam as a function of tin content.[34] With an increase in tin content, the critical amorphization temperature gradually decreased from 666 K for $Y_2Sn_{0.4}Ti_{1.6}O_7$ to 251 K for the $Y_2Sn_{1.2}Ti_{0.8}O_7$, hence suggesting the increased radiation resistance of the Sn-rich pyrochlore system.[34] In addition, Lian *et al.* investigated the

radiation response of stannate pyrochlores ($RE_2Sn_2O_7$; RE = La–Lu and Y) to a 1 MeV Kr^{2+} ion beam and determined the effect of the size of the A-site cations on their radiation stability.[33] Stannate pyrochlores with larger A-site cations (La, Nd, Gd) can be amorphized at room temperature and have critical temperatures of amorphization in the range of 350–960 K.[33] However, materials with smaller A-site cations (Y, Er) cannot be amorphized even at 25 K and transform to a defect fluorite structure.[33]

Several studies in the literature have performed ion-irradiation experiments on single phase crystalline pyrochlore ceramics. However, to the best of our knowledge, very few studies exist on the ion-irradiation of titanate pyrochlore GCs and no studies exist for stannate pyrochlore GCs.[36] Also, the structural response of pyrochlores with 1 : 1 Ti : Sn content ($LnTiSnO_7$) to ion irradiation has not been investigated. Previous ion-irradiation studies on stannate pyrochlores have been performed using Kr ions, which are relatively light compared to a typical heavy recoil nucleus and it is known from the literature that the amorphization dose is dependent on the ion mass.[33,34,37] Therefore, in this study, the Sn-substituted pyrochlore GCs ($Y_2Ti_{2-x}Sn_xO_7$ and Ln_2TiSnO_7) were irradiated using 600 keV heavier Xe^{2+} ions and the structural response was monitored *in situ* using transmission electron microscopy (TEM). The primary goals of this study were to determine the effects of Sn-content ($Y_2Ti_{2-x}Sn_xO_7$; $0 \leq x \leq 2$), A-site cations (Ln_2TiSnO_7; RE = Er, Y, Gd, Sm, and Nd), ion-mass, and temperature on the radiation response of Sn-substituted pyrochlore glass GCs.

2. Experimental

2.1. Synthesis of $Y_2Ti_{2-x}Sn_xO_7$ and Ln_2TiSnO_7 GC

The $Y_2Ti_{2-x}Sn_xO_7$ ($0 \leq x \leq 2$) and Ln_2TiSnO_7 (Ln = Er, Y, Gd, Sm, Nd) GC samples were synthesized *via* a soft chemistry route followed by high temperature sintering treatment. The detailed synthetic procedure is discussed in the previous studies.[38,39] All the starting chemicals (A. R. Grade) used in this study were purchased from Sigma-Aldrich (Merck). Powders of glass ($Na_2AlBSi_6O_{16}$) were synthesized *via* heat-treatment of a mixture of the following precursors at 550 °C for 3 h: Na_2CO_3 (99.5%+), Al_2O_3 (99.5%+), H_3BO_3, and SiO_2 (99.9%+). The ceramic component was synthesized using a coprecipitation route in which tin(IV) chloride pentahydrate (98%+) was dissolved in water before adding to an oxalate solution (prepared by dissolving oxalic acid (98%+) in water) and the pH of the resulting mixture was adjusted to 7.0–7.2 *via* dropwise addition of 1.667 M ammonia. The resulting precipitate was separated and washed and dried before resuspending in water *via* sonication. Subsequently, calculated amounts of lanthanide(III) nitrate hexahydrate (99.8%+) and Tyzor LA (titanium(IV) bis(ammonium lactate)dihydroxide solution; 50 wt% in water) were added to the Sn-containing mixture and thoroughly stirred before drying at 100 °C. Then, the Ln–Ti–Sn oxide powder mixture was heated at 700 °C for 6 h in air. The GC samples were produced by mixing the Ln–Ti–Sn oxide powder with the glass powder in 4 : 6 glass to ceramic weight ratio, followed by pressing the powder into pellets (11 mm diameter) at 180 MPa and subsequently heating at 1200 °C in air for 4 h. The as-sintered pellets had a diameter of ~10 mm and a thickness of ~2–3 mm.

2.2. Powder XRD

The phase purity and crystal structure of the as-synthesized $Y_2Ti_{2-x}Sn_xO_7$ and Ln_2TiSnO_7 GCs were determined by collecting powder XRD patterns using a PANalytical X'pert Pro Diffractometer (Almelo, the Netherlands) equipped with a Cu Kα radiation source (λ_{ave} = 1.541847 Å; 45 kV and 40 mA). The as-synthesized GCs were ground manually to fine powders and the XRD patterns were collected from these powders in the range of 10° to 80° (step size = 0.008°, acquisition time/step = 2 s). The lattice constants of the materials were determined using the HighScore Plus software program.[40]

2.3. *In situ* ion irradiation

Thin specimens for TEM analysis were obtained by crushing the powders of as-synthesized GCs in ethanol, followed by placing a drop of the solution on a 3 mm copper TEM grid coated with a holey carbon film. The as-prepared TEM grids were mounted on a Gatan double tilt heating (DTH) holder (for experiments at or above room temperature), and the bright-field TEM images and selected area diffraction patterns (SAED) were collected using a Hitachi H-9500 TEM and a 300 keV electron beam. The TEM images and SAED patterns were analyzed using the ImageJ, FIJI software.[41,42] *In situ* ion irradiation of GCs was performed at the MIAMI-2 facility at the University of Huddersfield, UK.[43] At the MIAMI-2 facility, the ion-accelerator (350 kV National Electrostatics Corporation equipped with a Danfysik 921A ion source) is coupled to a TEM (Hitachi H-9500 TEM) and this experimental setup allows the user to monitor the changes in the material as a function of ion-irradiation under real-time conditions.[43] The ion irradiation was performed using 600 keV Xe^{2+} ions over a wide range of temperatures (103–973 K). For ion irradiation experiments below room temperature (~27 °C = 300 K), the TEM sample grids were mounted on a Gatan liquid nitrogen cooled TEM holder. The sample temperature was maintained using temperature controllers (SmartSet Models 900/901 hot/cold stage controller). It is to be noted that prior to ion-irradiation, the sample was allowed to dwell at the desired temperature for ~10–15 min to minimize inhomogeneity in sample temperature. The Xe^{2+} ion beam incident on the sample has a spot size of 1 mm and the Xe^{2+} ion flux was experimentally determined at the sample location (error bar: ±10%) before and after the ion irradiation experiment using a current measuring rod (CMR)/Faraday cup. The ion-irradiation experiments were performed over several weeks and hence, the Xe^{2+} ion flux cannot be held constant at a particular value, although the order of magnitude was held constant throughout the experiment. In this study, ion-irradiation of GCs was performed using a Xe^{2+} flux of ~1.2×10^{12} to 4.3×10^{12} ions cm^{-2} s^{-1}. The ion irradiation was performed in incremental time steps to monitor the

structural response of materials at different ion fluences. It should be noted that throughout the experiment, the electron beam was turned off during the ion irradiation to eliminate electron beam-induced recrystallization of the sample.

The displacement per atom (dpa) values corresponding to the various ion-fluences were calculated using the stopping and range of ions in matter (SRIM) software.[44] The dpa values shown in this study correspond to the dpa value from the near surface region ($\sim$30 nm). The calculation was performed using a total of 5000 ions in full damage cascade mode and the angle of incidence of the ion-beam (600 keV Xe^{2+}) with respect to the target surface was 18.7°. The displacement energy (E_d) of all the atoms was set at 40 eV and the values of the density of the samples used in the calculation were determined using the lattice parameters. For comparison of the results from ion-irradiation using Xe and Kr ions, the nuclear stopping powers $\left(\frac{dE}{dx}\right)_n$ of 600 keV Xe^{2+} and 1 MeV Kr^{2+} ions in $Y_2Ti_2O_7$ and $Y_2Sn_2O_7$ were calculated using SRIM software.[44]

3. Results and discussion

3.1. Crystal structure: powder XRD

The cation ionic radius ratio (r_A/r_B) is useful in determining the structure of $A_2B_2O_7$ materials.[19] The pyrochlore structure has r_A/r_B values between 1.46 and 1.78, while the defect fluorite-type structure has $r_A/r_B < 1.46$.[19] In this study, both $Y_2Ti_{2-x}Sn_xO_7$ and Ln_2TiSnO_7 GC samples have r_A/r_B values within the range expected for a pyrochlore crystal system (Table 1). The lattice parameters were obtained by performing a Rietveld refinement of the XRD data. Analysis of the powder XRD patterns of the as-synthesized GC samples ($Y_2Ti_{2-x}Sn_xO_7$ and Ln_2TiSnO_7) also shows that the ceramic phase adopts the pyrochlore structure (Fig. 2 and Table 1). Small amounts of SnO_2 were found to be present in the Sn-rich compositions (*i.e.*, x = 1.6 and 2) of $Y_2Ti_{2-x}Sn_xO_7$ samples (Fig. 2a).[39] Similarly, minor amounts of SnO_2 and rutile-TiO_2 were present in the powder XRD pattern of Nd_2TiSnO_7 (Fig. 2b).[38]

In the $Y_2Ti_{2-x}Sn_xO_7$ series, the diffraction peaks were found to gradually shift to lower 2θ values with an increasing Sn-content because of an increase in the unit cell constants and volumes (see Fig. 2 and Table 1). This observation indicates the incorporation of a larger Sn ion on the pyrochlore B-site and the formation of the solid solutions in the entire compositional range, as highlighted by the linear relation between the composition 'x' and unit cell constants' 'a (Å)' and unit cell volume V (Å^3) (Fig. 3a). For pyrochlore materials with 1 : 1 Ti : Sn content (Ln_2TiSnO_7), a similar trend was observed in that the unit cell constants and unit cell volumes of the material were found to linearly increase as a function of Ln^{3+} ionic radii (Table 1 and Fig. 3b).

Table 1 Unit cell constants of $Y_2Ti_{2-x}Sn_xO_7$ and Ln_2TiSnO_7 GCs

Composition	Ionic radius (Å)	Radius ratio (r_A/r_B)	Unit cell, a (Å)
$Y_2Ti_2O_7$	$Y^{(VIII)}$ = 1.019 $Ti^{(VI)}$ = 0.605	1.68	10.0988 (1)
$Y_2Ti_{1.6}Sn_{0.4}O_7$	$Sn^{(VI)}$ = 0.69	1.63	10.1586 (1)
$Y_2Ti_{0.4}Sn_{1.6}O_7$	—	1.51	10.3276 (1)
$Y_2Sn_2O_7$	—	1.48	10.3752 (1)
Er_2TiSnO_7	$Er^{(VIII)}$ = 1.004	1.55	10.2307 (2)
Y_2TiSnO_7	$Y^{(VIII)}$ = 1.019	1.57	10.2521 (2)
Gd_2TiSnO_7	$Gd^{(VIII)}$ = 1.053	1.62	10.3450 (3)
Sm_2TiSnO_7	$Sm^{(VIII)}$ = 1.079	1.66	10.3958 (8)
Nd_2TiSnO_7	$Nd^{(VIII)}$ = 1.109	1.71	10.4652 (4)

3.2. Xe^{2+} ion-irradiation of $Y_2Ti_{2-x}Sn_xO_7$ GCs

The effect of incorporation of Sn into the B-site of the pyrochlore structure on their radiation response was investigated and some of the representative SAED patterns of the pristine and ion-irradiated $Y_2Ti_{2-x}Sn_xO_7$ (x = 0, 0.4, 1, 1.6, and 2) collected at 143 K are presented in Fig. 4. All the compositions undergo a crystalline to amorphous transformation upon ion-irradiation at 143 K. However, a significant increase in the critical amorphization fluences, F_c (*i.e.*, the fluence at which a complete loss of diffraction maxima is observed in the SAED pattern) of $Y_2Ti_{2-x}Sn_xO_7$ is noticed with an increase in Sn-content. The Ti-rich compositions (x = 0 and 0.4) are amorphized at a much lower Xe^{2+} ion fluence in comparison to their Sn-rich counterparts (x = 1.6 and 2) and there is approximately one order of magnitude difference in the value of F_c between the Ti- and Sn-end members (Table 2). The relatively large value of F_c for Sn-rich samples suggests that the Sn-rich pyrochlores are more radiation tolerant than Ti-rich pyrochlores. Similar observations about the varied structural response of Ti- and Sn-rich pyrochlores were made by Lumpkin *et al.* in a study in which the $Y_2Ti_{2-x}Sn_xO_7$ (x = 0.4, 0.8, 1.2, 1.6) ceramics were irradiated with higher energy but lighter ions (1 MeV Kr^{2+}).[34] It was reported that Sn-rich pyrochlores exhibited superior radiation performance when compared to the Ti-rich system and that the sample with composition x = 1.6 remained crystalline up to 5 × 10^{15} ions per cm^2 at 50 K.[34] In the present study, the sample with x = 1.6 got amorphized (F_c = 1.3 × 10^{15} ions per cm^2) at 143 K, albeit at a higher amorphization fluence and the differences in experimental observations between the two studies are primarily attributed to changes in the mass and energy of the ions used for irradiation. These observations highlight that the heavier ions are more effective at radiation-induced amorphization in materials than the lighter ions.

The radiation response of these ceramics was also studied as a function of temperature to evaluate the value of T_c and F_c. The general trend is that the F_c of the $Y_2Ti_{2-x}Sn_xO_7$ system increases as a function of temperature and Sn-content. However, at a certain temperature termed as critical temperature (T_c), the materials do not transform to the amorphous state anymore and continue to remain crystalline throughout. The T_c is dependent on the composition of the material as well as the mass and energy of the ions used for irradiation. In this study, a large decrease in the value of T_c was observed as a function of Sn content. For example, in the case of the $Y_2Ti_2O_7$ system, the materials underwent radiation-induced amorphization up to 823 K and at 893 K, the material did not undergo amorphization and remained crystalline up to a maximum fluence of

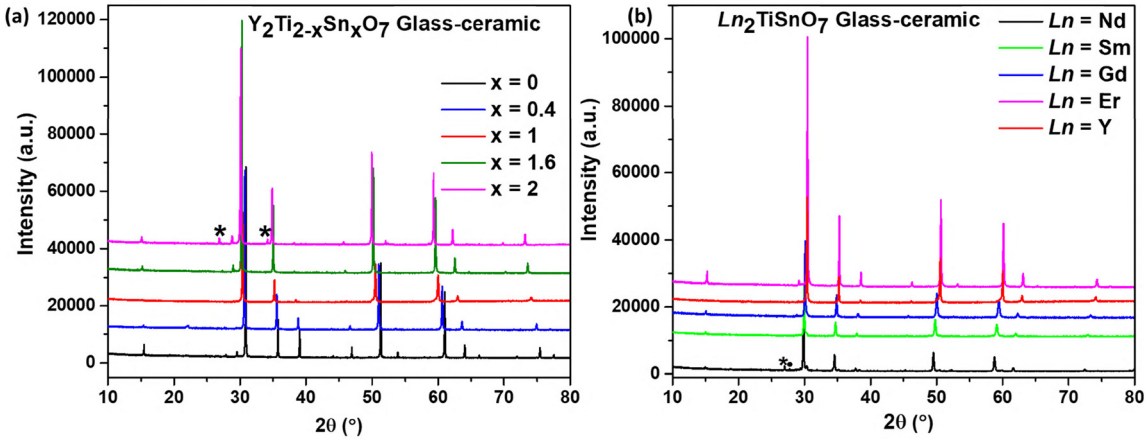

Fig. 2 (a) Powder XRD pattern of $Y_2Ti_{2-x}Sn_xO_7$ (x = 0, 0.4, 1, 1.6, and 2.0). Minor quantities of SnO_2 (indicated by *) were observed in Sn-rich compositions (x = 1.6 and 2.0). (b) Powder XRD pattern of Ln_2TiSnO_7 (Ln = Er, Y, Gd, Sm, and Nd) GCs. Minor quantities of SnO_2 (indicated by *) and rutile-TiO_2 (indicated by ●) were observed in the powder XRD pattern of Nd_2TiSnO_7.

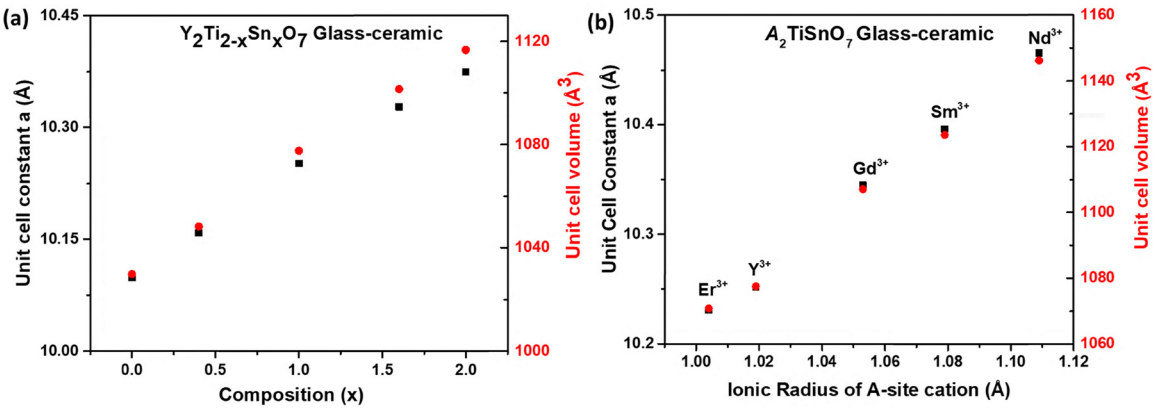

Fig. 3 Plots of (a) unit cell constant (and unit cell volume) *vs.* composition for $Y_2Ti_{2-x}Sn_xO_7$ GCs and (b) unit cell constant (and unit cell volume) *vs.* ionic radius of the A-site cation for Ln_2TiSnO_7 GC.

1.18×10^{15} ions per cm^2. For $Y_2Sn_2O_7$, the material underwent amorphization from 103.15 K up to room temperature (~298 K). Beyond room temperature, at 348 K, the material remained crystalline even up to a fluence of 1.8×10^{16} ions per cm^2. The exact value of T_c lies between the temperature at which the amorphization was fully observed and the next highest temperature at which the material remained crystalline, thus providing the lower and upper limits of T_c. The experimentally measured T_c, as reported in Table 3, was determined by taking the average of these two temperatures. Hence, the T_c of $Y_2Ti_2O_7$ and $Y_2Sn_2O_7$ are ~858 K and ~323 K, respectively. Therefore, a ~3-fold decrease in the T_c was observed when the B-site of the pyrochlore structure was completely substituted by Sn for Ti.

For the quaternary solid-solutions, the decrease in the T_c was also observed with increased Sn-doping on the pyrochlore Ti-site. The T_c of samples with x = 0.4, 1, and 1.6 are 783 K, 423 K, and 323 K, respectively. The critical amorphization fluences of the $Y_2Ti_{2-x}Sn_xO_7$ system are plotted as a function of temperature and is presented in Fig. 5. The T_c of the samples was also determined by fitting the non-linear curve using eqn (1) and by using the experimentally determined temperature limits, as mentioned earlier, as constraints.[34]

$$F_c = \frac{F_{c,0}}{1 - \exp\left[\left(\frac{E_a}{k_B}\right)\left(\frac{1}{T_c} - \frac{1}{T}\right)\right]} \quad (1)$$

In eqn (1), F_c denotes the critical amorphization fluence at temperature T, $F_{c,0}$ is the amorphization fluence at 0 K evaluated from the fitting procedure, E_a is the activation energy for the recrystallization of the radiation-damaged zones, k_B is the Boltzmann constant, T_c is the critical temperature, and T is the temperature at which the ion-irradiation experiment was carried out. The curve fitting was done by allowing the $F_{c,0}$, E_a, and T_c to vary.

The values of T_c, $F_{c,0}$, and E_a obtained from the fit are presented in Table 3 along with the T_c values determined by taking averages from the temperatures at which 'amorphization'

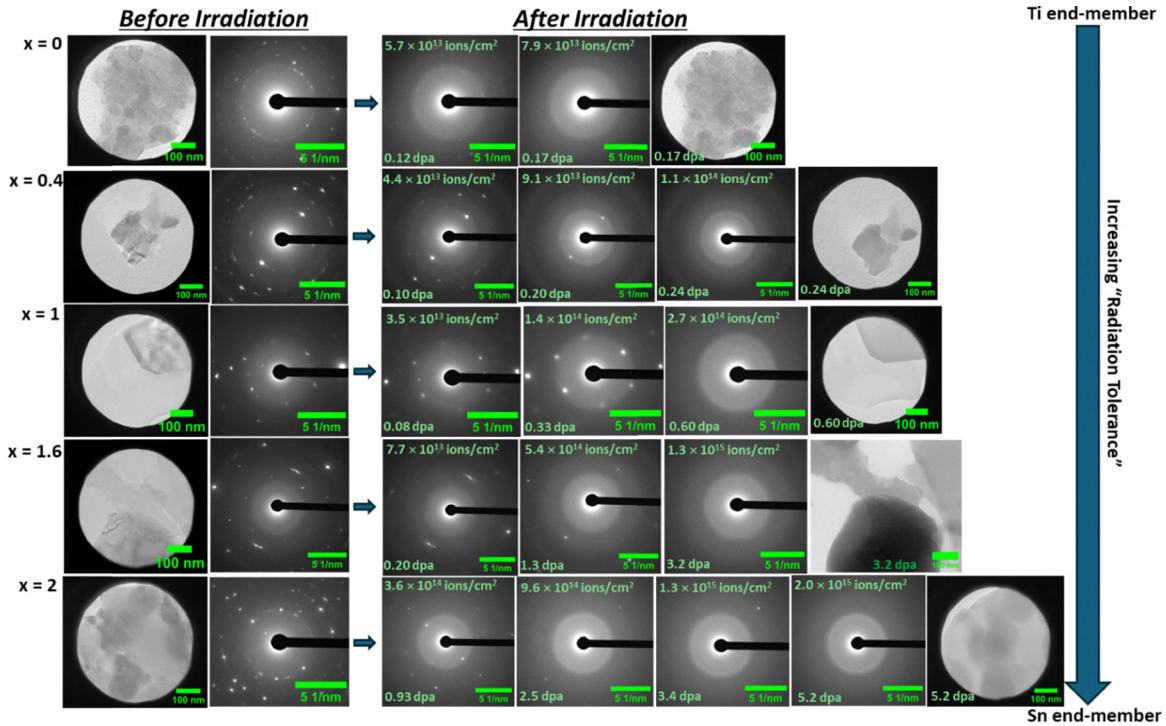

Fig. 4 SAED patterns of pristine and Xe^{2+} ion-irradiated $Y_2Ti_{2-x}Sn_xO_7$ GCs at −130 °C (143 K). The critical amorphization fluences (F_c in ions per cm^2) and the dpa increases with an increase in Sn-substitution, thus indicating the greater radiation tolerance of Sn-rich samples.

Table 2 Critical amorphization fluence (F_c) of $Y_2Ti_{2-x}Sn_xO_7$ at 143 K

Composition, x	Critical amorphization fluence, F_c (ions per cm^2)
0	7.9×10^{13}
0.4	1.1×10^{14}
1	2.7×10^{14}
1.6	1.3×10^{15}
2	2×10^{15}

Table 3 Critical amorphization temperature, T_c, of $Y_2Ti_{2-x}Sn_xO_7$

Composition, x	T_c (K) (curve-fit)	T_c (K) (experiment)	$F_{c,0}$ (ions per cm^2)	E_a (eV)
0	918 (6)	858	$1.5\ (2.7) \times 10^{14}$	0.253 (0.0878)
0.4	762 (14)	783	$1.6\ (3.6) \times 10^{14}$	0.452 (0.322)
1	401 (1)	423	$2.7\ (3.2) \times 10^{14}$	0.214 (0.001)
1.6	320 (9)	323	$6.2\ (3.5) \times 10^{14}$	0.023 (0.021)
2	380 (18)	323	$8.2\ (5.8) \times 10^{14}$	0.010 (0.008)

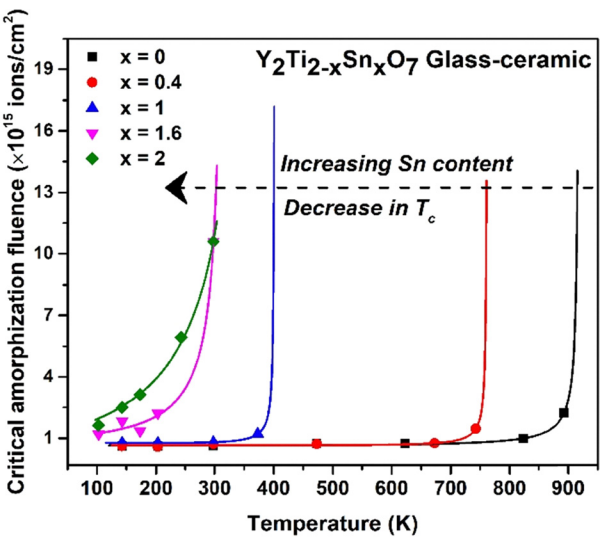

Fig. 5 Plot of critical amorphization fluence (F_c) *versus* temperature for the $Y_2Ti_{2-x}Sn_xO_7$ GCs. The T_c was found to decrease with an increase in Sn-substitution.

and 'no amorphization' events were observed. A large decrease in the T_c was observed with an increase in Sn-content and it should be noted that the radiation response of Sn-rich (x = 1.6) and Sn-end member (x = 2) samples is almost similar, with both these samples having similar T_c values. Like F_c, the values of $F_{c,0}$ were also observed to increase with an increase in the Sn-content and indicate an increase in the radiation tolerance. The E_a values are low for all the samples, and it has been indicated in a study by Meldrum *et al.* that the E_a values determined from the fitting of curves have significant error and hence, their physical meaning is rather limited.[45] However, it was suggested that the E_a values could be used for comparative purposes and in this study, the general trend is that the E_a values decrease with an increase in Sn-content.[45] A comparison is given at 143 K and 298 K in Fig. 6 to highlight the increase in the radiation tolerance of these materials with an increase in tin content. With an increase in Sn-content, there is an increase in the F_c and is accompanied by a decrease in

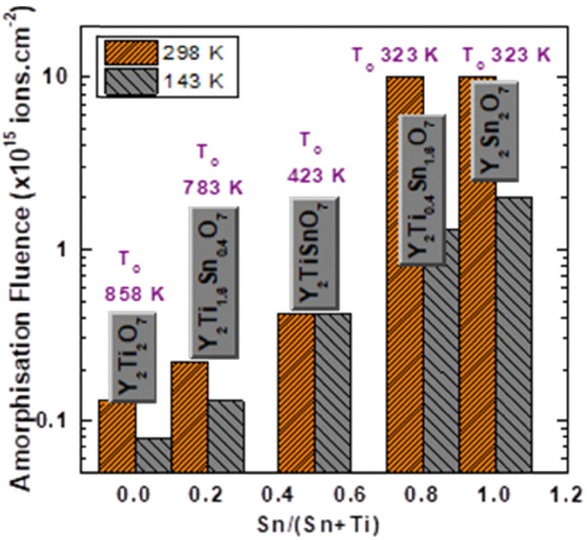

Fig. 6 Comparison of the radiation response of $Y_2Ti_{2-x}Sn_xO_7$ materials at 298 K and 143 K. With an increase in Sn-content, the materials become more radiation tolerant.

the T_c. Using the values of F_c, the Sn-end member was determined to be ~25 times and ~78 times more radiation tolerant than its Ti-counterpart at 143 K and 298 K, respectively (Table 2).

For a waste form, the material should have greater radiation tolerance and lower T_c. The Sn-rich pyrochlores fulfill both these criteria, and it is worth noting here that the T_c of samples with compositions $x \geq 1$ lie within the temperatures expected in a geological repository (320–400 K).[31] Therefore, in a geological repository, Sn-rich materials can be expected to better resist radiation-induced crystalline to amorphous transformation and can help offset detrimental effects, such as waste form swelling and concomitant decrease in chemical durability.

3.3. Xe^{2+} ion-irradiation of Ln_2TiSnO_7 GC

The effect of variation in the sizes of the A-site cations (Ln = Er, Y, Gd, Sm, and Nd) on the radiation response of pyrochlores with a fixed 1 : 1 Ti : Sn content was also investigated. Representative SAED patterns of pristine and ion-irradiated Ln_2TiSnO_7 materials collected at 298 K are presented in Fig. 7. All the materials exhibited similar radiation response and became amorphous at fluences ranging from 1.2×10^{14} to 9.1×10^{14} ions per cm^2. No significant trends in the values of F_c were observed with variations in the ionic radius of the A-site cations.

The radiation response of Ln_2TiSnO_7 was also studied as a function of temperature to determine the T_c. The plots of F_c *versus* temperature of Ln_2TiSnO_7 materials are presented in Fig. 8 and the curves were fitted using eqn (1) to determine the T_c for Nd_2TiSnO_7, Gd_2TiSnO_7, and Y_2TiSnO_7. For Sm_2TiSnO_7 and Er_2TiSnO_7, the fit did not converge due to the lack of enough experimental data points and hence, the T_c of these

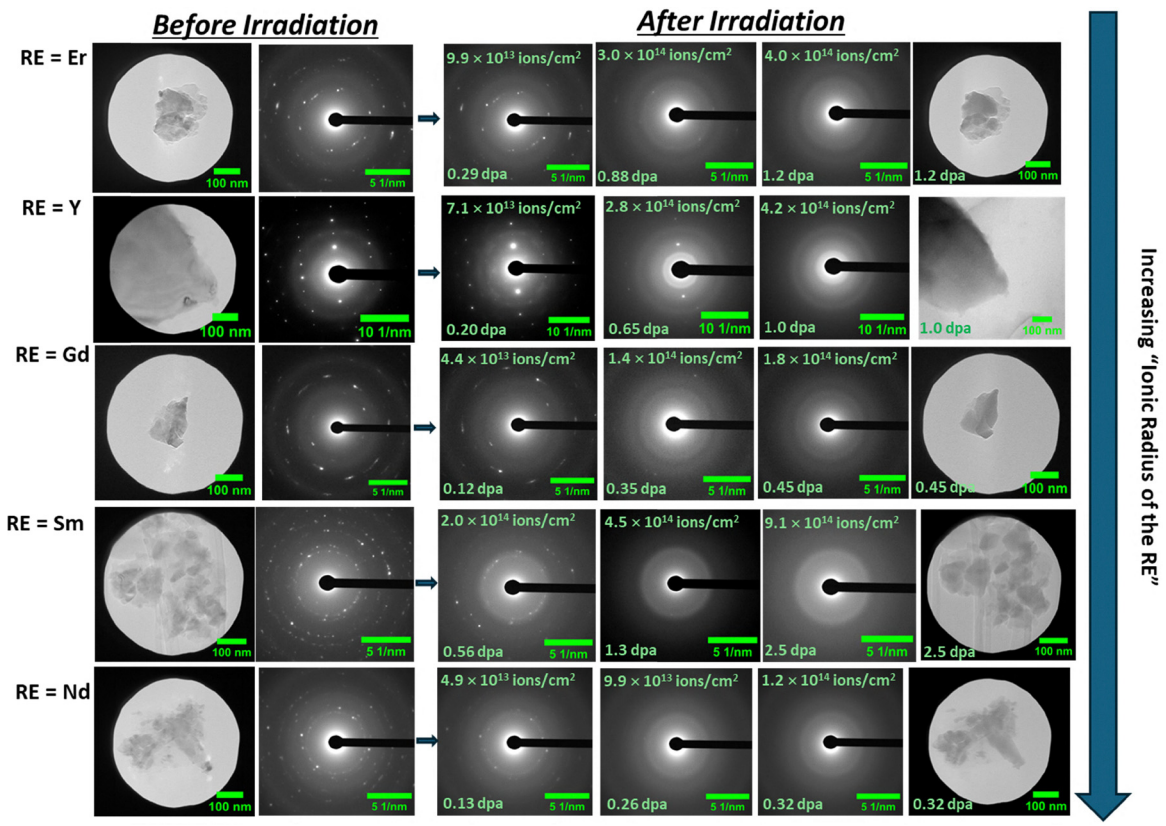

Fig. 7 SAED patterns of pristine and Xe^{2+} ion-irradiated Ln_2TiSnO_7 (Ln = Er, Y, Gd, Sm, and Nd) GCs at 298 K. No significant trends in the F_c and dpa were observed with variations in the ionic radius of the RE ion.

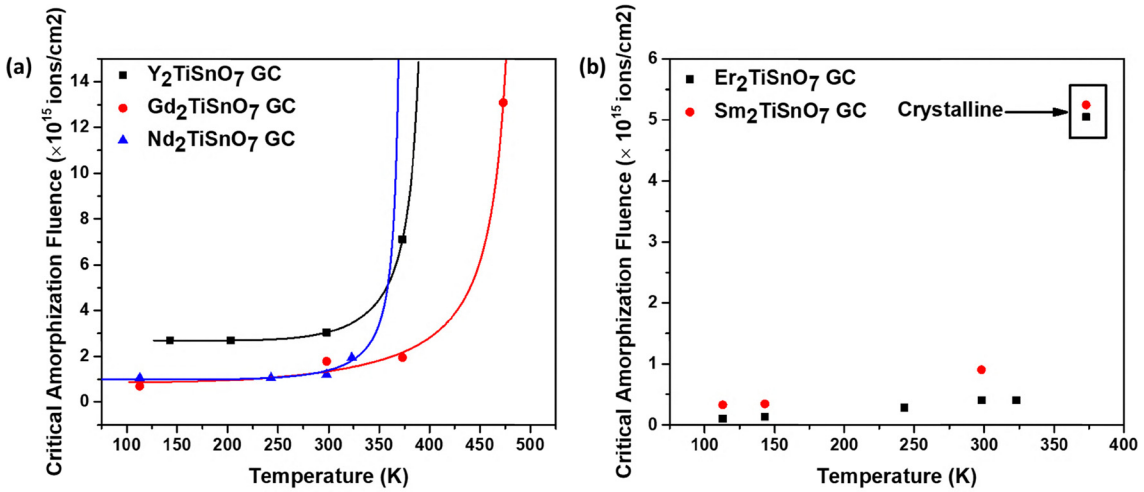

Fig. 8 (a) Plot of F_c *versus* temperature for Y_2TiSnO_7, Gd_2TiSnO_7, and Nd_2TiSnO_7 GCs. The T_cs of these materials were determined by fitting the data points using eqn (1). (b) Plot of F_c *versus* temperature for Sm_2TiSnO_7 and Er_2TiSnO_7 GC. Due to the lack of sufficient data points, the fitting was not performed for these two materials. This plot also indicates the data collected at 373 K, wherein the material remained crystalline at all fluences.

materials was determined from the average of temperatures at which the amorphization was fully observed and the next highest temperature at which the material remained crystalline. The values of T_c are presented in Table 4 and no trends could be observed with variations in the sizes of the A-site cations. The T_c's for Ln_2TiSnO_7 varied from ~336 to 523 K depending on the composition and are much lower when compared to the T_c of Ti-pyrochlore. Since changing the A-site cation in Ln_2TiSnO_7 does not significantly impact the radiation tolerance of the material, these materials could offer flexibility in accepting a variable waste feedstock. From a radiation stability perspective, Ln_2TiSnO_7 pyrochlores are more suitable for use as a host matrix in repository environments in comparison to a titanate pyrochlore.

3.4. Xe^{2+} *vs.* Kr^{2+} ion-irradiation of $Y_2Ti_{2-x}Sn_xO_7$

The effect of varying the ion mass and energy on the radiation response of $Y_2Ti_{2-x}Sn_xO_7$ is discussed in this section. The values of F_c (at room temperature) and T_c obtained in the present study using heavier 600 keV Xe^{2+} ions are compared to those obtained in the studies by Lumpkin *et al.* and Lian *et al.* using a relatively lighter 1 MeV Kr^{2+} ions (Table 5).[33,34] The Xe^{2+} ions have a higher atomic mass than the Kr^{2+} ions and hence, they are expected to simulate more closely the heavier α-recoil nuclei formed during the α-decay of actinides.

It is observed that for both Xe^{2+} and Kr^{2+} irradiated samples, the trends in the value of F_c and T_c with an increase in Sn-content are similar (Table 5). Both experiments indicated that the Sn-rich pyrochlores are more radiation tolerant than the Ti-rich pyrochlores. However, a comparison between Xe^{2+} and Kr^{2+} irradiated samples indicated that the value of F_c for Xe^{2+} irradiated $Y_2Ti_2O_7$ and $Y_2Ti_{1.6}Sn_{0.4}O_7$ samples is relatively lower, while the value of T_c is relatively higher than the Kr^{2+} irradiated samples. This observation can be explained by considering the nuclear stopping powers (*i.e.*, energy loss occurring due to elastic collisions of energetic ions with the target atoms in the material) of Xe^{2+} and Kr^{2+} ions.[46] It must be noted that the nuclear stopping powers are both energy- and mass-dependent. For instance, the nuclear stopping powers $\left(\frac{dE}{dx}\right)_n$ of 600 keV Xe^{2+} and 1 MeV Kr^{2+} ions in $Y_2Ti_2O_7$ are 3.2 keV nm^{-1} and 1.3 keV nm^{-1}, respectively. The higher stopping power of Xe^{2+} ions indicates that a greater number of elastic collisions occur per unit path length, thereby creating more collision cascades. As a result, the heavier Xe^{2+} ions produce more defects in the material than the Kr^{2+} ions, thereby rendering the material amorphous at relatively lower ion-fluences and thus has a lower F_c than the Kr^{2+} irradiated materials. The relatively higher density of defects in Xe^{2+} irradiated materials would also indicate that more thermal energy would be required for their recombination, and hence the T_c for these experiments is higher than the Kr^{2+} irradiated materials. The comparisons between Xe and Kr ion-irradiation experiments thus indicate that the values of F_c and T_c are dependent on the energy and mass of the ions used in irradiation.

Table 4 Critical amorphization temperature, T_c, of Ln_2TiSnO_7

Ln	T_c (K) (curve-fit)	T_c (K) (experiment)	$F_{c,0}$ (ions per cm^2)	E_a (eV)
Er	—	348	—	—
Y	401 (1)	423	2.7 (3.2) × 10^{14}	0.214 (0.001)
Gd	493 (9)	523	8.5 (5.1) × 10^{13}	0.065 (0.060)
Sm	—	336	—	—
Nd	339 (1)	348	1.0 (9.0) × 10^{14}	0.448 (0.033)

3.5. Further discussion: radiation tolerance of Sn- *vs.* Ti-pyrochlores

Ion irradiation of $Y_2Ti_{2-x}Sn_xO_7$ has revealed that F_c increases with an increase in Sn content, while T_c decreases with an increase in Sn content. These observations highlight the decreased susceptibility of Sn-rich pyrochlores to radiation-induced

Table 5 Comparison of F_c (room temperature) and T_c values of $Y_2Ti_{2-x}Sn_xO_7$ obtained using Xe^{2+} (this study) and Kr^{2+} (Lumpkin *et al.*[34] and Lian *et al.*[33]) ion irradiation

	This study – 600 keV Xe^{2+}		Literature – 1 MeV Kr^{2+}	
Samples	F_c (ions per cm^2)	T_c (K)	F_c (ions per cm^2)	T_c (K)
$Y_2Ti_2O_7$	1.3×10^{14}	858	4×10^{14}	780
$Y_2Ti_{1.6}Sn_{0.4}O_7$	2.2×10^{14}	783	6.4×10^{14}	666
$Y_2Ti_{1.2}Sn_{0.8}O_7$	No data	No data	2.3×10^{15}	335
Y_2TiSnO_7	4.2×10^{14}	423	No data	No data
$Y_2Ti_{0.8}Sn_{1.2}O_7$	No data	No data	No data[a]	251
$Y_2Ti_{0.4}Sn_{1.6}O_7$	1.01×10^{16}	323	Crystalline up to 5×10^{15} [b]	No data
$Y_2Sn_2O_7$	1.01×10^{16}	323	Crystalline up to 6.25×10^{15} [b]	No data

[a] The F_c value at 200 K for the Kr^{2+} irradiated $Y_2Ti_{0.8}Sn_{1.2}O_7$ sample is 2.0×10^{15} ions per cm^2. [b] No amorphization observed for Kr^{2+} irradiated $Y_2Ti_{0.4}Sn_{1.6}O_7$ and $Y_2Sn_2O_7$ samples.

amorphization. The differing radiation response of Ti-rich *vs.* Sn-rich pyrochlores could be attributed to a result of the complex interplay of structure, energetics, and bond-type variations in these materials and will be discussed in this section.

Several ion-irradiation studies on titanate pyrochlores (*e.g.*, $Gd_2Ti_2O_7$) have shown that these materials could be easily amorphized at relatively low ion fluences.[47] In these studies, it was shown that they initially undergo a radiation-induced transformation from an ordered pyrochlore to a disordered fluorite structure and subsequently transform to an amorphous state.[47] The zirconate pyrochlores (*e.g.*, $Gd_2Zr_2O_7$), on the other hand, have also been shown to initially transform to the defect fluorite structure upon irradiation but continue to remain crystalline even at higher ion-fluences.[47] The varying radiation response of these two pyrochlores is attributed to the stability of the intermediate defect fluorite phase.[47] Sickafus *et al.* determined using atomistic simulation methods that materials with significantly dissimilar ionic radii of A and B site cations require higher energy to form the defect fluorite phase.[26] In $Gd_2Ti_2O_7$, the ionic radius of Gd and Ti are widely different and hence the radiation-induced formation of intermediate defect fluorite phase is metastable and readily transforms to a stable amorphous state on further irradiation.[47] It was also shown by Sickafus *et al.* that materials with similar ionic radii of A and B cations require lower energy to form the defect fluorite phase and were shown to be stable in radiation environments.[26] In $Gd_2Zr_2O_7$, the Gd and Zr have similar ionic radii and hence, the intermediate defect fluorite structure is stable and resists amorphization.[47]

In the present study, the $Y_2Ti_{2-x}Sn_xO_7$ materials adopt the ordered pyrochlore structure at all compositions and the A- and B-site cations are occupied by Y and Ti (and/or Sn), respectively. However, with an increase in Sn content, the radius ratio of A to B-site cations decreases from 1.68 ($Y_2Ti_2O_7$) to 1.48 ($Y_2Sn_2O_7$) and approaches the value of $\frac{r_A}{r_B}$ to <1.46 necessary to form the defect fluorite structure in which the cationic anti-site disorder occurs between the A and B-sites. Based on the conclusions obtained in the study by Sickafus *et al.*, it is proposed that the Sn-rich pyrochlores would require relatively lower energy to form the intermediate defect fluorite phase upon irradiation and hence, the Sn-rich defect fluorite phase is energetically more stable than the Ti-rich defect fluorite phase.[26] The Sn-rich defect fluorite phase can also accommodate further radiation-induced point defects (*e.g.*, vacancies and interstitials) within the disordered structure and as a result, these materials have higher critical amorphization fluences than the Ti-pyrochlores.[26] Similarly, the lower critical temperatures of Sn-rich pyrochlores are attributed to the increased stabilization of the defect fluorite structure and recombination of point defects at $\sim$ 323 K.

Helean *et al.* found a correlation between the radiation response of titanate pyrochlores ($Ln_2Ti_2O_7$; Ln = Sm–Lu and Y) to 1 MeV Kr^+ ions and their thermodynamic stability as indicated by their enthalpies of formation from oxides ($\Delta H^\circ_{f\text{-}ox}$ in kJ mol^{-1}).[48] It was shown in that study that the critical amorphization temperature, T_c, of titanate pyrochlores decreases with a decrease in the ionic radius of the A-site cation.[48] The T_c decreases from 1120 K for $Gd_2Ti_2O_7$ to 480 K for $Lu_2Ti_2O_7$.[48] A similar trend was observed for $\Delta H^\circ_{f\text{-}ox}$ *i.e.*, the values of $\Delta H^\circ_{f\text{-}ox}$ become less negative with a decrease in A-site radii.[48] The values of $\Delta H^\circ_{f\text{-}ox}$ for $Gd_2Ti_2O_7$ and $Lu_2Ti_2O_7$ are -113.4 kJ mol^{-1} and -56 kJ mol^{-1}, respectively.[48] The less negative value of $\Delta H^\circ_{f\text{-}ox}$ for $Lu_2Ti_2O_7$ indicates that the thermodynamic stability of the Lu-pyrochlore is relatively lower than Gd-pyrochlore and hence, shows an increased propensity to transform to an energetically favorable defect fluorite structure upon irradiation.[48] As a result, the Lu-pyrochlore with a lower T_c exhibited better radiation tolerance than the Gd-pyrochlore.[48]

Similarly, Lian *et al.* determined the $\Delta H^\circ_{f\text{-}ox}$ of stannate pyrochlores ($Ln_2Sn_2O_7$; Ln = La, Nd, Sm, Eu, Dy, Yb) and their radiation response to 1 MeV Kr^{2+} ions.[33] Like titanate pyrochlores, the $\Delta H^\circ_{f\text{-}ox}$ of $Ln_2Sn_2O_7$ becomes less negative with a decrease in A-site radii, thereby suggesting a decrease in the thermodynamic stability of the pyrochlore structure on moving from $La_2Sn_2O_7$ to $Yb_2Sn_2O_7$.[33,48] This decrease in thermodynamic stability could explain the decrease in T_c from 960 K for $La_2Sn_2O_7$ to 350 K for $Gd_2Sn_2O_7$.[33] In the present study, the increased radiation tolerance of Sn-rich pyrochlores could also be understood using the $\Delta H^\circ_{f\text{-}ox}$ values reported by Helean *et al.* and Lian *et al.*[33,48] Helean *et al.* experimentally determined the

$\Delta H^{\circ}_{f\text{-}ox}$ of $Y_2Ti_2O_7$ to be −86.2 (1.5) kJ mol^{-1} while Lian *et al.* determined the $\Delta H^{\circ}_{f\text{-}ox}$ of $Dy_2Sn_2O_7$ and $Yb_2Sn_2O_7$ to be −53.57 (3.06) kJ mol^{-1} and −37.99 kJ mol^{-1}, respectively.[33,48] It must be noted that the $\Delta H^{\circ}_{f\text{-}ox}$ for $Y_2Sn_2O_7$ was not determined by Lian *et al.* and since the ionic radius of the Y ion is between the ionic radius of Dy and Yb ions it is assumed in this study that the $\Delta H^{\circ}_{f\text{-}ox}$ for $Y_2Sn_2O_7$ is between −53.57 kJ mol^{-1} and −37.99 kJ mol^{-1}.[33] The $Y_2Sn_2O_7$ material has a less negative value of $\Delta H^{\circ}_{f\text{-}ox}$ than the $Y_2Ti_2O_7$ material, which suggests that the Sn-pyrochlores are less thermodynamically stable than the Ti-pyrochlores. This observation suggests the increased propensity for Sn-rich pyrochlores to transform to an energetically stable defect fluorite structure upon irradiation and as a result, the Sn-rich pyrochlores have a higher F_c and a lower T_c than the Ti-rich pyrochlores.

Some studies in the literature have also explained the susceptibility of pyrochlore materials to amorphization using the nature of the A–O and B–O bond in $A_2B_2O_7$ materials.[33,49,50] In a study by Panero *et al.*, first principles calculations on $Y_2(Ti,Sn,Zr)_2O_7$ pyrochlores have revealed that the Sn–O bond is more covalent than the Ti–O and Zr–O bonds, whereas the Y–O bond is ionic. It was indicated in that study, the greater degree of covalency in the Sn–O bond promoted an increase in the energy required to form a defect fluorite structure. As indicated previously in a study by Sickafus *et al.*, a higher defect-formation energy for a material would indicate a decreased propensity to form defect-fluorite structure and thus, a lower resistance to radiation.[26] Based on the correlation between bond-type and radiation response, it is expected that stannate pyrochlores with a covalent Sn–O bond should experience more radiation damage than titanate and zirconate pyrochlores.[51] However, experimentally, it is observed in the present study, as well as in the studies by Lian *et al.* and Lumpkin *et al.*, that the $Y_2Sn_2O_7$ materials have a better radiation tolerance compared to the $Y_2Ti_2O_7$ material.[33,34] This observation reveals that the complex radiation behaviour of stannate pyrochlores cannot be explained wholly by using a single factor such as the bond type. Rather, a combination of the three factors, namely cation ionic radius ratio, bond-type, and energetics, should be used in explaining the radiation behaviour of these materials.[33] It is proposed in this study that the variations in the radiation response of $Y_2Ti_{2-x}Sn_xO_7$ with an increase in Sn-content are a result of different degrees of contribution from each of the three factors discussed above.

3.6. Implications

Titanate pyrochlores have been considered as candidate waste forms for immobilising excess plutonium and actinide-rich radioactive wastes.[4] However, their poor radiation resistance should be appropriately addressed to achieve their full potential in nuclear waste management.[19,22,23] It seems that the issue can be well resolved by partial Zr/Sn-substitution for Ti.[26,33,34] Although improved radiation tolerance has been demonstrated by Zr/Sn-substitution of Ti in titanate pyrochlore, both zirconate and stannate pyrochlores require high sintering temperatures and are porous in full ceramics due to their finer grain size.[4,39,52,53] This limits their real applications as ceramic waste forms for actinide immobilisation. However, the developed GC waste forms have some important implications. The addition of glass in the GC waste forms significantly lowers the processing temperature, making such practical applications possible. In addition, such advanced GCs are also ideal waste forms for plutonium residue wastes and many actinide-rich waste streams arising from the nuclear fuel cycle. However, it must be noted that synthesizing Zr-rich pyrochlore in a glass-ceramic is inherently difficult since high temperatures of 1600 °C are required to form the ceramic phase. In comparison, the Sn-rich pyrochlore GC can be synthesized at a much lower temperature of 1200 °C.

4. Conclusion

In this study, the effect of variations in the composition of the A-site and B-site of the pyrochlore system on their radiation stability was investigated *via in situ* ion-irradiation of the $Y_2Ti_{2-x}Sn_xO_7$ and Ln_2TiSnO_7 GC materials. Titanate pyrochlores ($Y_2Ti_2O_7$) were readily amorphized and were shown to have a higher critical amorphization temperature ($T_c \sim 858$ K); however, upon replacing the Ti with Sn, the critical amorphization fluence (F_c) increases and the materials become increasingly radiation resistant. A ∼3-fold decrease in the value of critical temperature (T_c) was observed when the Ti was fully replaced with Sn ($T_c \sim 323$ K). In the case of Ln_2TiSnO_7 GC materials, no systematic trends in the amorphization fluence and critical temperature of amorphization were observed; however, these materials also have a lower T_c when compared to the titanate pyrochlores. The study also showed that the values of T_c are relatively higher for a heavy ion such as Xe used in our study, compared to the previously known values determined using the lighter Kr ions. It was shown in this study that the radiation tolerance of the pyrochlore materials could be improved through Sn-substitution in the B-site of the pyrochlore structure and that the value of T_c lies within the temperatures expected in a geological repository (320–400 K). Further ion-irradiation studies on these materials using heavier ions such as Au ions could provide more insight into their radiation tolerance, given that the ion mass was shown to have a measurable impact on the values of T_c and F_c. This study has demonstrated the suitability of Sn-doped pyrochlore glass-ceramic as a potential waste form for the immobilization of actinides (in the ceramic phase) and processing impurities (in the glass phase) found in the HLW stream.

Conflicts of interest

There are no conflicts to declare.

Data availability

All the data supporting the findings of this study are available within this article.

Acknowledgements

Material synthesis and characterisation were carried out in the facilities under the Nuclear Materials Research and Technology Group at ANSTO. The *in situ* ion-irradiation was performed at the MIAMI-2 facility (EP/M028283/1) in the University of Huddersfield, Huddersfield, UK. MRR and AHM acknowledge the financial support provided by the EPSRC through the EPSRC Early Career Fellowship Grant (EP/T012811/1) awarded to AHM.

References

1 A. Slameršak, G. Kallis and D. W. O'Neill, *Nat. Commun.*, 2022, **13**, 6932.
2 R. C. Ewing, *Nat. Mater.*, 2015, **14**, 252–257.
3 D. J. Gregg, J. S. McCloy, J. D. Vienna, A. M. Macfarlane, W. J. Weber and G. R. Lumpkin, *Bull. At. Sci.*, 2025, **81**, 3–16.
4 R. C. Ewing, W. J. Weber and J. Lian, *J. Appl. Phys.*, 2004, **95**, 5949–5971.
5 Y. Zhang, L. Kong, M. Ionescu and D. J. Gregg, *J. Eur. Ceram. Soc.*, 2022, **42**, 1852–1876.
6 Y. Zhang, Z. Zhang, G. Thorogood and E. R. Vance, *J. Nucl. Mater.*, 2013, **432**, 545–547.
7 R. Farzana, Y. Zhang, P. Dayal, Z. Aly, R. Holmes, G. Triani, E. R. Vance and D. J. Gregg, *J. Eur. Ceram. Soc.*, 2021, **41**, 7269–7281.
8 Y. Zhang, Z. Zhang, T. Wei, L. Kong, Y. J. Kim and D. J. Gregg, *J. Am. Ceram. Soc.*, 2020, **103**, 5470–5479.
9 M. Lang, F. Zhang, J. Zhang, J. Wang, J. Lian, W. J. Weber, B. Schuster, C. Trautmann, R. Neumann and R. C. Ewing, *Nucl. Instrum. Methods Phys. Res., Sect. B*, 2010, **268**, 2951–2959.
10 F. P. Marlton, Z. Zhang, Y. Zhang, T. E. Proffen, C. D. Ling and B. J. Kennedy, *Chem. Mater.*, 2021, **33**, 1407–1415.
11 A. Navrotsky, *J. Mater. Chem.*, 2005, **15**, 1883–1890.
12 T. M. Nenoff, D. X. Rademacher, M. A. Rodriguez, T. J. Garino, T. Subramani and A. Navrotsky, *J. Solid State Chem.*, 2021, **299**, 122163.
13 L. Kong, Z. Zhang, M. de los Reyes, I. Karatchevtseva, G. R. Lumpkin, G. Triani and R. D. Aughterson, *Ceram. Int.*, 2015, **41**, 5309–5317.
14 K. Momma and F. Izumi, *J. Appl. Crystallogr.*, 2011, **44**, 1272–1276.
15 W. J. Weber, R. C. Ewing, C. R. A. Catlow, T. D. de la Rubia, L. W. Hobbs, C. Kinoshita, H. Matzke, A. T. Motta, M. Nastasi, E. K. H. Salje, E. R. Vance and S. J. Zinkle, *J. Mater. Res.*, 1998, **13**, 1434–1484.
16 S. V. Yudintsev, A. A. Lizin, T. S. Livshits, S. V. Stefanovsky, S. V. Tomilin and R. C. Ewing, *J. Mater. Res.*, 2015, **30**, 1516–1528.
17 R. C. Ewing, J. Lian and L. M. Wang, *MRS Online Proc. Libr.*, 2003, **792**, 190–201.
18 R. P. Turcotte, J. W. Wald, F. P. Roberts, J. M. Rusin and W. Lutze, *J. Am. Ceram. Soc.*, 1982, **65**, 589–593.
19 J. Shamblin, C. L. Tracy, R. C. Ewing, F. Zhang, W. Li, C. Trautmann and M. Lang, *Acta Mater.*, 2016, **117**, 207–215.
20 J. W. Wald and P. Offemann, *MRS Online Proc. Libr.*, 2011, **11**, 369.
21 G. S. Was and R. S. Averback, in *Comprehensive Nuclear Materials*, ed. R. J. M. Konings, Elsevier, Oxford, 2012, pp. 195–221, DOI: 10.1016/B978-0-08-056033-5.00007-0.
22 J. Lian, J. Chen, L. M. Wang, R. C. Ewing, J. M. Farmer, L. A. Boatner and K. B. Helean, *Phys. Rev. B:Condens. Matter Mater. Phys.*, 2003, **68**, 134107.
23 J. Lian, W. J. Weber, W. Jiang, L. M. Wang, L. A. Boatner and R. C. Ewing, *Nucl. Instrum. Methods Phys. Res., Sect. B*, 2006, **250**, 128–136.
24 E. R. Aluri and A. P. Grosvenor, *J. Alloys Compd.*, 2014, **616**, 516–526.
25 K. E. Sickafus, R. W. Grimes, J. A. Valdez, A. Cleave, M. Tang, M. Ishimaru, S. M. Corish, C. R. Stanek and B. P. Uberuaga, *Nat. Mater.*, 2007, **6**, 217–223.
26 K. E. Sickafus, L. Minervini, R. W. Grimes, J. A. Valdez, M. Ishimaru, F. Li, K. J. McClellan and T. Hartmann, *Science*, 2000, **289**, 748–751.
27 E. C. O'Quinn, D. L. Drey and M. K. Lang, *Front. Chem.*, 2021, **9**, 733718.
28 G. R. Lumpkin, K. R. Whittle, S. Rios, K. L. Smith and N. J. Zaluzec, *J. Phys.: Condens. Matter*, 2004, **16**, 8557.
29 J. Lian, L. M. Wang, J. Chen, R. C. Ewing and K. V. G. Kutty, *MRS Proc.*, 2002, **713**, JJ11.35.
30 S. X. Wang, B. D. Begg, L. M. Wang, R. C. Ewing, W. J. Weber and K. V. G. Kutty, *J. Mater. Res.*, 1999, **14**, 4470–4473.
31 R. C. Kale and K. Ravi, *Environ. Technol. Innovation*, 2021, **23**, 101728.
32 Z.-T. Zhao, R.-F. Guo, H.-R. Mao and P. Shen, *J. Eur. Ceram. Soc.*, 2021, **41**, 5768–5773.
33 J. Lian, K. B. Helean, B. J. Kennedy, L. M. Wang, A. Navrotsky and R. C. Ewing, *J. Phys. Chem. B*, 2006, **110**, 2343–2350.
34 G. R. Lumpkin, K. L. Smith, M. G. Blackford, K. R. Whittle, E. J. Harvey, S. A. T. Redfern and N. J. Zaluzec, *Chem. Mater.*, 2009, **21**, 2746–2754.
35 S. V. Yudintsev, S. V. Tomilin, T. S. Livshits, A. A. Lizin and I. A. Goryatchev, *Dokl. Earth Sci.*, 2016, **469**, 732–736.
36 M. Jiang, A. Haq Mir, M. Bahri, Y. Zhang, N. Browning, K. Whittle and M. Patel, *J. Nucl. Mater.*, 2023, **581**, 154424.
37 L. M. Wangl, R. C. Ewing, W. J. Weber and R. K. Eby, *MRS Online Proc. Libr.*, 1992, **279**, 451–456.
38 L. Kong, I. Karatchevtseva and T. Wei, *J. Nucl. Mater.*, 2023, **577**, 154322.
39 L. Kong, I. Karatchevtseva and T. Wei, *J. Am. Ceram. Soc.*, 2023, **106**, 3141–3154.
40 T. Degen, M. Sadki, E. Bron, U. König and G. Nénert, *Powder Diffr.*, 2014, **29**, S13–S18.
41 J. Schindelin, I. Arganda-Carreras, E. Frise, V. Kaynig, M. Longair, T. Pietzsch, S. Preibisch, C. Rueden, S. Saalfeld, B. Schmid, J.-Y. Tinevez, D. J. White, V. Hartenstein, K. Eliceiri, P. Tomancak and A. Cardona, *Nat. Methods*, 2012, **9**, 676–682.
42 C. A. Schneider, W. S. Rasband and K. W. Eliceiri, *Nat. Methods*, 2012, **9**, 671–675.

43 G. Greaves, A. H. Mir, R. W. Harrison, M. A. Tunes, S. E. Donnelly and J. A. Hinks, *Nucl. Instrum. Methods Phys. Res., Sect. A*, 2019, **931**, 37–43.
44 J. F. Ziegler, M. D. Ziegler and J. P. Biersack, *Nucl. Instrum. Methods Phys. Res., Sect. B*, 2010, **268**, 1818–1823.
45 A. Meldrum, L. A. Boatner and R. C. Ewing, *Phys. Rev. B:Condens. Matter Mater. Phys.*, 1997, **56**, 13805–13814.
46 T. Zagyva, A. H. Mir, L. Leay, B. O'Driscoll, M. Harrison, T. Taylor and R. W. Harrison, *Acta Mater.*, 2023, **261**, 119391.
47 J. Lian, L. Wang, J. Chen, K. Sun, R. C. Ewing, J. Matt Farmer and L. A. Boatner, *Acta Mater.*, 2003, **51**, 1493–1502.
48 K. B. Helean, S. V. Ushakov, C. E. Brown, A. Navrotsky, J. Lian, R. C. Ewing, J. M. Farmer and L. A. Boatner, *J. Solid State Chem.*, 2004, **177**, 1858–1866.
49 E. R. Aluri and A. P. Grosvenor, *Phys. Chem. Chem. Phys.*, 2013, **15**, 10477–10486.
50 E. R. Aluri, J. R. Hayes, J. D. S. Walker and A. P. Grosvenor, *J. Phys. Chem. C*, 2014, **118**, 7910–7922.
51 W. R. Panero, L. Stixrude and R. C. Ewing, *Phys. Rev. B:Condens. Matter Mater. Phys.*, 2004, **70**, 054110.
52 B. Matovic, J. Maletaskic, J. Zagorac, V. Pavkov, R. S. S. Maki, K. Yoshida and T. Yano, *J. Eur. Ceram. Soc.*, 2020, **40**, 2652–2657.
53 A. F. Fuentes, E. C. O'Quinn, S. M. Montemayor, H. Zhou, M. Lang and R. C. Ewing, *Appl. Phys. Rev.*, 2024, **11**, 021337.